AIP Advances

Spin Hall effect and current induced magnetic switching in antiferromagnetic IrMn

Cite as: AIP Advances **8**, 115323 (2018); https://doi.org/10.1063/1.5059386
Submitted: 20 September 2018 • Accepted: 12 November 2018 • Published Online: 21 November 2018

Lijuan Qian, Wenzhe Chen, Kang Wang, et al.

View Online

Export Citation

CrossMark

ARTICLES YOU MAY BE INTERESTED IN

Spin transfer torque devices utilizing the giant spin Hall effect of tungsten
Applied Physics Letters **101**, 122404 (2012); https://doi.org/10.1063/1.4753947

The design and verification of MuMax3
AIP Advances **4**, 107133 (2014); https://doi.org/10.1063/1.4899186

Recent advances in spin-orbit torques: Moving towards device applications
Applied Physics Reviews **5**, 031107 (2018); https://doi.org/10.1063/1.5041793

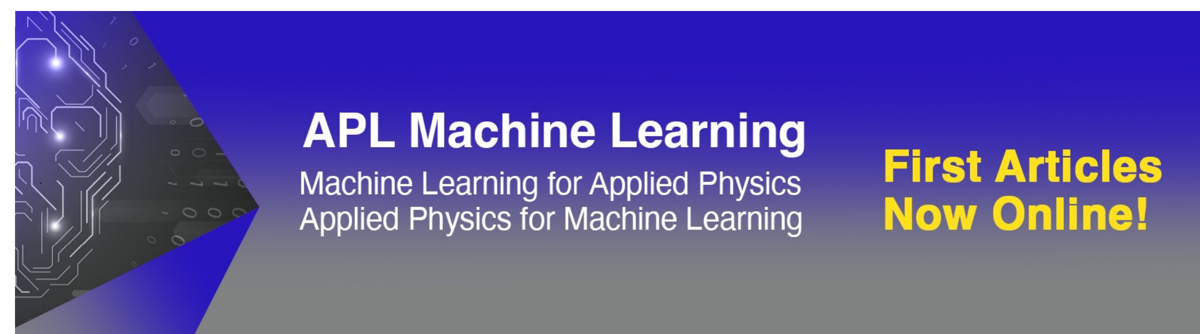

© 2018 Author(s).

AIP ADVANCES **8**, 115323 (2018)

Spin Hall effect and current induced magnetic switching in antiferromagnetic IrMn

Lijuan Qian,[1] Wenzhe Chen,[1] Kang Wang,[2] Xiaoshan Wu,[2] and Gang Xiao[1,a]
[1]*Department of Physics, Brown University, Providence, Rhode Island 02912, USA*
[2]*Collaborative Innovation Center of Advanced Microstructures, Laboratory of Solid State Microstructures, School of Physics, Nanjing University, Nanjing 210093, China*

(Received 20 September 2018; accepted 12 November 2018; published online 21 November 2018)

An antiferromagnetic metal (AFM) rich in spin-orbit coupling is a promising solid for the application of electrical current induced magnetic switching, because not only can it rely on its Spin Hall Effect (SHE) to generate spin current, it might also provide exchange coupling field to replace an external field required for coherent magnetic switching. In this work, we study the current induced magnetic switching by using the antiferromagnetic IrMn. The switching current density based on the spin Hall effect of IrMn is on the order of $1\text{x}10^6$ A/cm^2, which is comparable to the heavy metal systems with a large spin Hall angle. We observe an interesting switching behavior, in that a complete binary switching occurs under an applied field in the range of 2.0 to 8.0 mT, however, from zero field up to 2.0 mT, switching is continuous and incomplete. We attribute this observation to the distribution of exchange bias field and the mixture of internal and external field, which is attested by magneto-optical Kerr effect microscope. Our study sheds light on the SHE in AFM materials and their application in field-free switching such as in spin-logic and magnetic random-access memory devices. © *2018 Author(s). All article content, except where otherwise noted, is licensed under a Creative Commons Attribution (CC BY) license (http://creativecommons.org/licenses/by/4.0/).* https://doi.org/10.1063/1.5059386

One of the recent breakthroughs in spintronics is the discovery of the spin Hall effect (SHE). This effect plays an important role in the development of the magnetic random-access memory and spin logic devices because of its ability to manipulate the magnetization through spin current.[1–5] Previous SHE studies are mainly focused on non-magnetic heavy metals (HMs), such as β-Ta, β-W, Pt, Hf etc.[4–13] HMs have large spin Hall angles ranging from 0.068 to 0.4.[4–10] Facilitated by an external field, the spin transfer torque generated from the HM is large enough to flip the magnetization of a perpendicularly magnetized layer between two stable states of spin-up and spin-down. In recent years, scientists have begun to turn their attention to the antiferromagnetic metals (AFMs) which also exhibit SHE.[14–25]

AFMs are well known in generating exchange bias field through exchange coupling with a ferromagnetic material (FM) in the AFM/FM bilayer structures.[26–31] The exchange anisotropy is discovered in Co with the shell of CoO and its bias field is as high as 0.2 T.[26] One famous application of AFM is to pin the magnetization vector of an ferromagnetic electrode and to form the so-called fixed layer in magnetic tunneling junctions.[32] Borrowing from the same idea, it is intuitive to use an AFM, which exhibits SHE, to provide the exchange biasing field needed for coherent magnetic switching. This dual functionality of an AFM simplifies SHE-based device structures and improves their energy efficiency.[16–18,25] Moreover, AFMs, such as PtMn, IrMn, PdMn, and FeMn, have considerable spin-orbit coupling[22–24] and they possess spin Hall angles ranging from 0.008 to 0.086.[15,19,20,22]

In this work, we study the magnetic switching behavior caused by the spin-transfer torque generated by the SHE of the antiferromagnetic IrMn, an important solid widely used in spintronic

[a]Email: Gang_Xiao@Brown.edu

 © Author(s) 2018

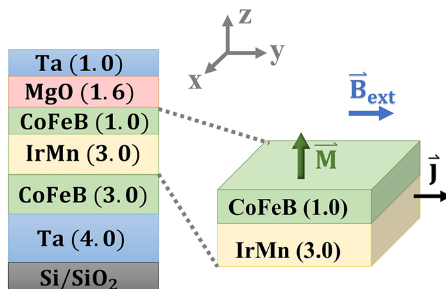

FIG. 1. Cross-sectional schematic view of our multilayer samples and schematic of the Hall resistance measurement set-up in our experiment. The number in the parentheses represents the layer thickness in nanometer. The external field and current are applied along the y-axis. The 1 nm-thick CoFeB has perpendicular magnetic anisotropy.

structures or devices. We observe a very low critical switching current density, even though the SHE in IrMn is moderate, compared with β-Ta and β-W.[5–8,13,15,20,22] Current-induced complete and sharp switchings occur upon a minimum external field of 2.0 mT. Yet, continuous and incomplete switching is observed under field-free condition and low applied fields up to 2.0 mT. We attribute this rather unique behavior in IrMn system to the polycrystalline morphology of the IrMn thin film, which yields a distribution of local biasing field across crystalline grains.

As illustrated in Fig. 1, the sample used in our study has the multilayer structure: Si-substrate/SiO_2/Ta(4.0)/CoFeB(3.0)/IrMn(3.0)/CoFeB(1.0)/MgO(1.6)/Ta(1.0), numbers denoting layer thicknesses in units of nanometer; IrMn and CoFeB standing for $Ir_{22}Mn_{78}$ and $Co_{40}Fe_{40}B_{20}$ alloys, respectively. We utilize a homemade sputtering system with a high vacuum base pressure of 2×10^{-8} Torr to grow the layered stack. The bottom Ta and CoFeB layers provide seed layers for the growth of IrMn. The IrMn has the dual roles of generating spin current and providing exchange biasing to the top 1.0-nm thick CoFeB. The proximity of MgO layer causes this CoFeB to exhibit a robust perpendicular magnetic anisotropy (PMA) after a careful magnetic annealing process. It is the perpendicular magnetic switching of this CoFeB layer that we will focus on, under the influence of the spin-transfer torque from IrMn and an external in-plane field. Finally, the top Ta layer acts as the capping layer to passivate the whole stack. We use standard photolithography to pattern the stack into Hall bars for magnetotransport measurements.

Fig. 2 shows the anomalous Hall resistance versus an out-of-plane magnetic field under different magnetic annealing conditions. The magnitude of the anomalous Hall resistance is proportional to the z-component of the magnetization vector of the 1 nm-thick CoFeB layer.[33] We anneal the samples under a perpendicular field (z-axis) of 0.42 T in a high vacuum chamber (2×10^{-6} Torr) at a fixed temperature ranging from 140 °C to 310 °C. We obtain a robust PMA as indicated by the square-like hysteresis loop in Fig. 2 only with a narrow temperature window around 150 °C. The corresponding

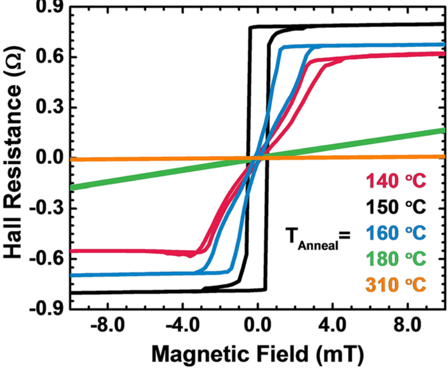

FIG. 2. Anomalous Hall resistance hysteresis loop under a sweeping perpendicular field for samples magnetically annealed at various temperatures.

coercivity is $H_c = 0.5$ mT. A small departure from 150 °C dampens the PMA, causing the magnetization vector to collapse to the in-plane state at 140 °C or 160 °C. It requires a critical field of 3.8 mT and 3.2 mT to bring the magnetization to be out-of-plane for the sample annealed at 140 °C and 160 °C, respectively. At and beyond 180 °C, PMA disappears completely, and the system is dominated by in-plane magnetic anisotropy. It would take a perpendicular field of 1.95 T to bring the magnetization to be out-of-plane. Going forward, we will present our measurement and analysis on the sample with natural PMA, which is annealed under the optimal condition, *i.e.*, 150 °C.

Next, we present the magnetic switching behavior of the 1.0-nm thick CoFeB under the excitation of a charge current and an in-plane external magnetic field, B_{ext}, schematically shown in Fig. 1. The value of current density presented refers to the IrMn layer. It is calculated considering different resistivity of each conducting layer using Eq. (1)[34]

$$j_{IrMn} = \left(\sum_i \frac{t_i}{\rho_i}\right)^{-1} \frac{I_{tot}}{\rho_{IrMn} w} \tag{1}$$

I_{tot} is the total current sent to the sample. $w = 20$ μm is the width of the Hall bar. t_i is the thickness of each conducting layer. ρ_i is the resistivity of each layer.[6,35] The magnetic state is detected by measuring the anomalous Hall resistance of the sample. Fig. 3(a) shows the hysteresis loops of Hall resistance within a current density range of ± 6.7 MA/cm^2, each under a fixed field B_{ext} (0.0, 0.5, 1.0, 2.0, 5.0 and 8.0 mT). Fig. 3(b) shows the same loops, except under various negative fixed fields.

An interesting observation in Fig. 3(a) and (b) is that, when $|B_{ext}| \geq 2.0$ mT, the perpendicular magnetic switching is complete and sharp. However, in the low field range of $0 < |B_{ext}| < 2.0$ mT, the switchings are gradual, nearly continuous, and incomplete. We can compare the two extreme conditions, switching at $B_{ext} = 8.0$ mT as shown in Fig. 3(c) and at zero field as shown in Fig. 3(d). In Fig. 3(c), we start the measurement with the current density sweeping from +6.7 MA/cm^2 to -6.7 MA/cm^2, and then reversing back to +6.7 MA/cm^2. The spin-down state with a low Hall resistance undergoes a switching to the spin-up state at the current density of -1.6 MA/cm^2, and in reversing, switching back to the spin-down state at the current density of 1.8 MA/cm^2. Between the binary stable states, the net change in the Hall resistance change is 1.46 Ω (100% switching). Fig. 3(e) and (g) shows the spin configuration of the binary states at -5 MA/cm^2 and +5 MA/cm^2 measured by magneto-optical Kerr effect (MOKE) microscope. The dark color in Fig. 3(e) and white color in Fig. 3(g) area are two single domain states, corresponding to spin-up and spin-down.

It is noteworthy that the critical switching current density (averaged at 1.7 MA/cm^2 under field above 2.0 mT) in the IrMn/CoFeB system is rather low. The switching current density is on the order of $10^6 \sim 10^7$ A/cm^2 in typical giant spin Hall effect multilayer systems.[5–7,15,36–38] The switching current density in our IrMn system is close to the lowest ones such as: 1.6 MA/cm^2 in β-W system in Q.Hao et al.'s work and ~1 MA/cm^2 in Ta system in S.Emori et al.'s work. However IrMn possesses a moderate spin Hall angle (SHA) of 0.02~0.06,[15,20,22] which is about one order of magnitude smaller than β-W and β-Ta. SHA reflects the efficiency of normal current to spin current conversion, which exerts a spin-transfer torque to switch the perpendicular magnetic moment. According to the work of K.Lee et al.,[39] the theoretical relation between the critical switching current density and spin Hall angle is,

$$J_C = \frac{2e}{\hbar} \frac{M_s t_F}{\theta_{SH}} \left(\frac{H_{K,eff}}{2} - \frac{H_y}{2}\right) \tag{2}$$

where J_c is the critical switching current density, M_s the saturation magnetization, t_F the thickness of switchable free layer, θ_{SH} the SHA, $H_{K,eff}$ the effective perpendicular anisotropy field, H_y the external field applied along the y-axis. Eq. (2) shows that the J_c is inversely proportional to the spin Hall angle. Given the relatively small SHA, one would expect a much larger J_c in this AFM/FM system than what is observed. The low current density arises possibly from a smaller $H_{K,eff}$ and a higher effective spin Hall angle. On one hand, the coupling between the AFM and the FM layer leads to a smaller $H_{K,eff}$ in Eq. (2) by providing an exchange bias to the FM layer. The PMA of the FM layer is more difficult to be established, in the sense that the required magnetic thermal annealing for the attainment of PMA is effective only within a narrow temperature window. The low coercivity at 0.5 mT as seen in Fig. 2 is also another evidence of the freely switchable FM layer. On the other hand, studies on the spin Hall effect of antiferromagnetic shows that the anti-damping torque is largely enhanced with

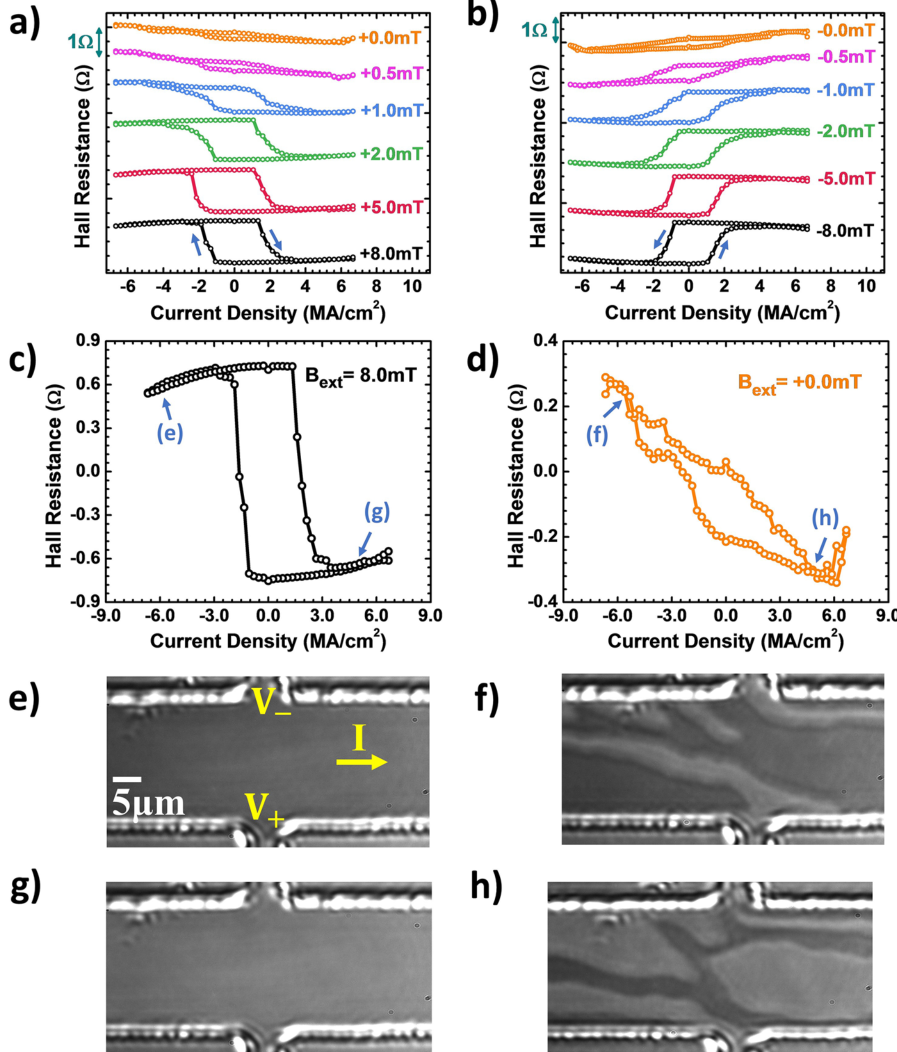

FIG. 3. (a) and (b): Hall resistance versus sweeping current density under different external field from ± 8.0 mT to ± 0.0 mT. The arrows represent the current sweeping direction. (c) and (d): Hall resistance versus sweeping current under external field +8.0 mT and 0.0 mT, respectively. (e) to (h): MOKE microscope image of magnetization configuration corresponding states labeled in (c) and (d).

an AFM/FM interface compared to those without such interface.[20,25] The effective spin Hall angle in IrMn is as large as 0.22±0.04. The possible mechanisms behind such enhancements are that the exchange coupling increases the spin current transparency and induces the additional toque directly from the interface.[20]

As mentioned earlier, when B_{ext} is reduced to zero, the FM switching becomes gradual, as shown in Fig. 3(d). Within the J_c range of ±6.7 MA/cm^2, the net change of Hall resistance is 0.62 Ω, compared with the net change of 1.46 Ω for a full switching shown in Fig. 3(c) under B_{ext} = 8.0 mT. Fig. 3(f) and 3(h) shows the MOKE spin configuration measured at ±5 MA/cm^2, respectively. Both states are multidomain states. In Fig. 4(a), red and green color area are the switchable domains with opposite switching directions by comparing Fig. 3(f) and (h). The rest area remains unchanged in the switching process.

There are two main reasons for the observed nearly continuous partial switching behavior near zero external field. First, it is due to the polycrystalline morphology[20] of the AFM IrMn, which is grown using the technique of magnetron sputtering. Such continuous switching is also observed in

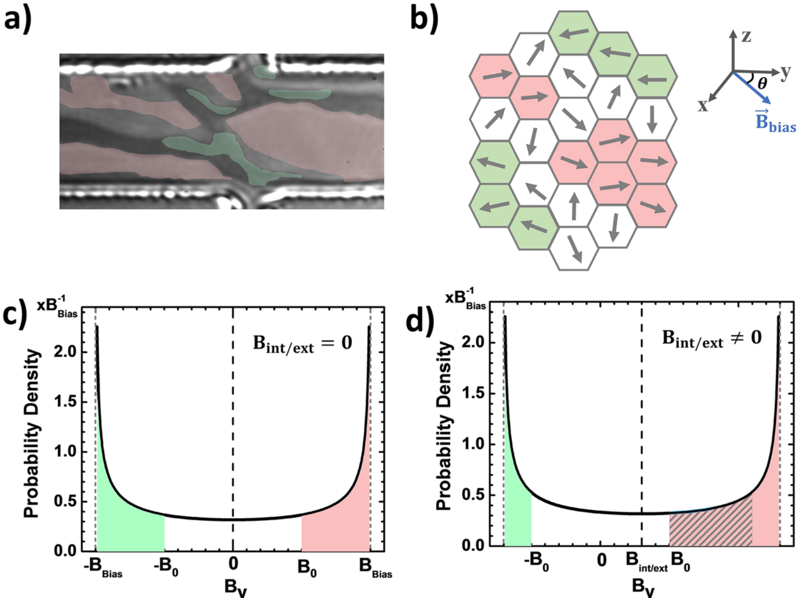

FIG. 4. (a) Comparison of MOKE images at ±5 MA/cm^2 under zero field (Fig. 3(f) and (g)). The red and green area represent domains favoring the opposite spin states under the same current. The rest area (light and dark gray) are not switchable in the switching process. (b) Schematic of a polycrystalline IrMn layer with local exchange biasing field pointing in random direction. θ is the angle between the exchange bias direction and the y-axis. (c) and (d) Probability density function of field along y-axis B_y when $B_{int/ext} = 0$ and $B_{int/ext} \neq 0$, respectively. The red area represents the grains that switches from spin-up to spin down states under a positive current. The green area represents the grains that switches from spin-down to spin-up states under a positive current. The dashed red area in (c) is the net switching area that can be measured through the Hall resistance.

other AFM-based systems[16,18] and it was found that the number of intermediate states decreases with the device size and vanishes when the dimension of the device is sub-micrometer.[14] The second reason is the distribution of exchange coupling between the IrMn and the CoFeB layer in different grains. In our experiment, the Néel point[26–28] of IrMn T_N, which is required for a unidirectional magnetic anisotropy, is higher than the optimal annealing temperature to obtain PMA in the top 1 nm-thick CoFeB layer. Annealed at $T < T_N$, the exchange biasing field is confined randomly within each IrMn crystalline grain.[40] In other words, the biasing field is local and its direction dispersive as illustrated in Fig. 4(b).

The effective field, coming from the exchange bias and internal/external field, plays the role for symmetry breaking and determines the switching direction of each grain. To quantitatively describe the effective field, we make the following assumptions:

a) the magnitude of the bias field within each grain is the same, denoted as B_{bias}.
b) the direction of the bias field within each grain is randomly distributed. The probability distribution function (PDF) of the angle between the bias field and y-axis is: $PDF(\theta) = \frac{1}{2\pi}$, $\theta \in [-\pi, \pi]$.
c) the switching of a grain happens when the effective field along y-axis within the grain is beyond a threshold B_0.
d) the field besides the exchange bias field along y-axis is $B_{int/ext}$, which includes both the applied external field and internal field generated from the structure.

Under these assumptions, the total field along the y-axis is given by $B_y = B_{bias}\, cos\,\theta + B_{int/ext}$ and the PDF of B_y through the probability transformation is as follow:

$$PDF(B_y = B_{bias}\, cos\,\theta + B_{int/ext}) = \frac{1}{\pi}\frac{1}{B_{bias}\sqrt{1-\left(\frac{B_y - B_{int/ext}}{B_{bias}}\right)^2}}, \quad B_y \in (-B_{bias}, B_{bias}) \tag{3}$$

Local magnetic switching occurs in grains when $|B_y| > B_0$. Under a sufficient positive current, the grains with $B_y > B_0$ would favor spin down states, and vice versa. The area of the red and green ones in Fig. 4(c) and Fig. 4(d) represents the number of grains switching in opposite direction. When $B_{int/ext} = 0$, switching in opposite directions cancels each other and macroscopically no switching is observed. When $B_{int/ext}$ is non-zero, the small internal or external field along y-axis breaks the symmetry of B_y as shown in Fig. 4(d). This would create an imbalance (the dashed red area) between grains favoring spin-up states (red area) and spin-down states (green area), which is consistent with our observation in Figure 4(a).

According to our models, the direction of switching is determined by the direction of $B_{int/ext}$. The switching at zero external field indicates the existence of a weak internal field besides the exchange bias in our system. The switching direction in Fig. 3(a) and Fig. 3(b) at zero external field shows that the direction of the field is history dependent and the same as the magnetization direction of the bottom CoFeB layer. One possible origin of such internal field is the "orange peel" coupling. According to the Néel model in trilayer systems, the magnitude of "orange peel" coupling field is given in Eq.(4).[41–43]

$$H_N = \frac{\pi^2}{\sqrt{2}}\left(\frac{h^2}{\lambda t_{FM}}\right)M_s e^{-2\sqrt{2}\pi t_{NM}/\lambda} \tag{4}$$

In our system, $t_{FM} = 1$nm and $t_{NM} = 3$nm are the thickness of the free ferromagnetic layer CoFeB and the non-magnetic layer IrMn, respectively. $h = 8.0$ Å and $\lambda = 98$ Å are the peak-to-peak amplitude and the wavelength of the sinusoidal roughness profile estimated from data and TEM images in literature.[42] $M_s = 848$ emu/cm^3 is the saturated magnetization of the free ferromagnetic layer. The Néel Field H_N is estimated to be 2.5 mT. In the high field range, the external field is large enough that B_y within all the grains are beyond B_0. All the grains switches in the same direction, leading to a transition from incomplete switching to complete switching at $B_{ext} = 2.0$mT in our experiment. According to Eq. (2), when $-B_{bias} + B_{int/ext} \geq B_0$, the switching becomes complete. B_{bias} is estimated to be < 4.5mT.

In conclusion, we study the current induced magnetic switching through the SHE in an FM/AFM/FM system (CoFeB/IrMn/CoFeB), from which we observe interesting magnetic switching behavior in the top CoFeB layer exhibiting PMA after proper magnetic thermal annealing. Under a high external field above 2.0 mT, the switching is complete and abrupt, and the required critical switching current density is low on the order of 10^6 A/cm^2, a benefit of the AFM. However, under zero or a low field less than 2.0 mT, the switching is incomplete and nearly continuous under a sweeping current. MOKE microscope image indicates the local dispersive exchange biasing fields within the crystalline grains of the AFM IrMn layer plays a role. Similar to other non-magnetic metals with SHE, antiferromagnetic alloys can also be employed as sources of spin current. One caveat is the random distribution of the local biasing field. Approaches to establish a net biasing field even at zero external field would lead to field-free current induced complete switchings in FM/AFM/FM systems. The "orange" coupling field, if sufficient, can be such an agent. Alternatively, AFMs with Néel point comparable with the optimal annealing temperature could be good candidates for this purpose.

The work was supported by National Science Foundation through Grants No. DMR-1307056, King Abdullah University of Science and Technology (KAUST), Nanoelectronics Research Initiative (NRI) through the Institute for Nanoelectronics Discovery and Exploration (INDEX), and the National Key R&D Program of China through Grant No. 2017YFA0303202.

[1] J. Hirsch, Phys. Rev. Lett. **83**, 091834 (1999).
[2] I. M. Miron, K. Garello, G. Gaudin, P. J. Zermatten, M. V. Costache, S. Auffret, S. Bandiera, B. Rodmacq, A. Schuhl, and P. Gambardella, Nature **476**, 189 (2011).
[3] J. Sinova, S. O. Valenzuela, J. Wunderlich, C. H. Back, and T. Jungwirth, Reviews of Modern Physics **87**, 1213 (2015).
[4] L. Liu, O. J. Lee, T. J. Gudmundsen, D. C. Ralph, and R. A. Buhrman, Phys. Rev. Lett. **109**, 096602 (2012).
[5] L. Liu, C. F. Pai, Y. Li, H. W. Tseng, D. C. Ralph, and R. A. Buhrman, Science **336**, 555 (2012).
[6] Q. Hao and G. Xiao, Phys. Rev. B **91**, 224413 (2015).
[7] Q. Hao and G. Xiao, Physical Review Applied **3**, 034009 (2015).
[8] C.-F. Pai, L. Liu, Y. Li, H. W. Tseng, D. C. Ralph, and R. A. Buhrman, Appl. Phys. Lett. **101**, 122404 (2012).
[9] C.-F. Pai, M.-H. Nguyen, C. Belvin, L. H. Vilela-Leão, D. C. Ralph, and R. A. Buhrman, Appl. Phys. Lett. **104**, 082407 (2014).
[10] Y. Wang, P. Deorani, X. Qiu, J. H. Kwon, and H. Yang, Appl. Phys. Lett. **105**, 152412 (2014).

[11] W. Chen, L. Qian, and G. Xiao, AIP Advances **8**, 055918 (2018).
[12] W. Chen, L. Qian, and G. Xiao, Scientific Reports **8**, 8144 (2018).
[13] Q. Hao, W. Chen, and G. Xiao, Appl. Phys. Lett. **106**, 182403 (2015).
[14] A. Kurenkov, C. Zhang, S. DuttaGupta, S. Fukami, and H. Ohno, Appl. Phys. Lett. **110**, 092410 (2017).
[15] D. Wu, G. Yu, C.-T. Chen, S. A. Razavi, Q. Shao, X. Li, B. Zhao, K. L. Wong, C. He, Z. Zhang, P. Khalili Amiri, and K. L. Wang, Appl. Phys. Lett. **109**, 222401 (2016).
[16] A. van den Brink, G. Vermijs, A. Solignac, J. Koo, J. T. Kohlhepp, H. J. Swagten, and B. Koopmans, Nat. Commun. **7**, 10854 (2016).
[17] W. J. Kong, Y. R. Ji, X. Zhang, H. Wu, Q. T. Zhang, Z. H. Yuan, C. H. Wan, X. F. Han, T. Yu, K. Fukuda, H. Naganuma, and M.-J. Tung, Appl. Phys. Lett. **109**, 132402 (2016).
[18] S. Fukami, C. Zhang, S. DuttaGupta, A. Kurenkov, and H. Ohno, Nat. Mater. **15**, 535 (2016).
[19] W. Zhang, M. B. Jungfleisch, F. Freimuth, W. Jiang, J. Sklenar, J. E. Pearson, J. B. Ketterson, Y. Mokrousov, and A. Hoffmann, Phys. Rev. B **92**, 144405 (2015).
[20] V. Tshitoyan, C. Ciccarelli, A. P. Mihai, M. Ali, A. C. Irvine, T. A. Moore, T. Jungwirth, and A. J. Ferguson, Phys. Rev. B **92**, 214406 (2015).
[21] H. Reichlová, D. Kriegner, V. Holý, K. Olejník, V. Novák, M. Yamada, K. Miura, S. Ogawa, H. Takahashi, T. Jungwirth, and J. Wunderlich, Phys. Rev. B **92**, 165424 (2015).
[22] W. Zhang, M. B. Jungfleisch, W. Jiang, J. E. Pearson, A. Hoffmann, F. Freimuth, and Y. Mokrousov, Phys. Rev. Lett. **113**, 196602 (2014).
[23] J. B. S. Mendes, R. O. Cunha, O. Alves Santos, P. R. T. Ribeiro, F. L. A. Machado, R. L. Rodríguez-Suárez, A. Azevedo, and S. M. Rezende, Phys. Rev. B **89**, 140406 (2014).
[24] H. Chen, Q. Niu, and A. H. MacDonald, Phys. Rev. Lett. **112**, 017205 (2014).
[25] Y. W. Oh, S. H. Chris Baek, Y. M. Kim, H. Y. Lee, K. D. Lee, C. G. Yang, E. S. Park, K. S. Lee, K. W. Kim, G. Go, J. R. Jeong, B. C. Min, H. W. Lee, K. J. Lee, and B. G. Park, Nat. Nanotechnol. **11**, 878 (2016).
[26] W. H. Meiklejohn and C. P. Bean, Physical Review **102**, 051413 (1956).
[27] A. Berkowitz and K. Takano, J. Magn. Magn. Mater. **200**, 552 (1999).
[28] K. O'Grady, L. Fernandez-Outon, and G. Vallejo-Fernandez, Journal of Magnetism and Magnetic materials **322**, 883 (2010).
[29] J. King, J. Chapman, M. Gillies, and J. Kools, J. Phys. D: Appl. Phys. **34**, 528 (2001).
[30] A. Malozemoff, J. Appl. Phys. **63**, 3874 (1988).
[31] J. Nogués and I. K. Schuller, J. Magn. Magn. Mater. **192**, 203 (1999).
[32] X. Liu, W. Zhang, M. J. Carter, and G. Xiao, J. Appl. Phys. **110**, 033910 (2011).
[33] N. Nagaosa, J. Sinova, S. Onoda, A. MacDonald, and N. Ong, Reviews of Modern Physics **82**, 1539 (2010).
[34] W. Chen, G. Xiao, Q. Zhang, and X. Zhang, Phys. Rev. B **98**, 134411 (2018).
[35] M. A. Seigler, Appl. Phys. Lett. **80**, 820 (2002).
[36] M. Akyol, W. Jiang, G. Yu, Y. Fan, M. Gunes, A. Ekicibil, P. Khalili Amiri, and K. L. Wang, Appl. Phys. Lett. **109**, 022403 (2016).
[37] S. Emori, U. Bauer, S. M. Ahn, E. Martinez, and G. S. Beach, Nat. Mater. **12**, 611 (2013).
[38] J. Han, A. Richardella, S. A. Siddiqui, J. Finley, N. Samarth, and L. Liu, Phys. Rev. Lett. **119**, 077702 (2017).
[39] K.-S. Lee, S.-W. Lee, B.-C. Min, and K.-J. Lee, Appl. Phys. Lett. **102**, 112410 (2013).
[40] M. Tsunoda and M. Takahashi, J. Appl. Phys. **87**, 6415 (2000).
[41] D. Wang, J. M. Daughton, Z. Qian, C. Nordman, M. Tondra, and A. Pohm, J. Appl. Phys. **93**, 8558 (2003).
[42] B. D. Schrag, A. Anguelouch, S. Ingvarsson, G. Xiao, Y. Lu, P. L. Trouilloud, A. Gupta, R. A. Wanner, W. J. Gallagher, P. M. Rice, and S. S. P. Parkin, Appl. Phys. Lett. **77**, 2373 (2000).
[43] W. Chen, L. Qian, and G. Xiao, Sci. Rep. **8**, 8144 (2018).